JACS
JOURNAL OF THE AMERICAN CHEMICAL SOCIETY
Article
pubs.acs.org/JACS

Hydrophobic Interaction Drives Surface-Assisted Epitaxial Assembly of Amyloid-like Peptides

Seung-gu Kang,[†] Tien Huynh,[†] Zhen Xia,[†] Yi Zhang,[‡,*] Haiping Fang,[‡] Guanghong Wei,[§] and Ruhong Zhou*[,†,⊥]

[†]Computational Biology Center, IBM Thomas J. Watson Research Center, Yorktown Heights, New York 10598, United States
[‡]Shanghai Institute of Applied Physics, Chinese Academy of Sciences, Shanghai 201800, China
[§]State Key Laboratory of Surface Physics, Key Laboratory for Computational Physical Sciences (Ministry of Education), and Department of Physics, Fudan University, 220 Handan Road, Shanghai, 200433, China
[⊥]Department of Chemistry, Columbia University, New York, New York 10027, United States

Supporting Information

ABSTRACT: The molecular mechanism of epitaxial fibril formation has been investigated for GAV-9 (NH_3^+-VGGAV-VAGV-$CONH_2$), an amyloid-like peptide extracted from a consensus sequence of amyloidogenic proteins, which assembles with very different morphologies, "upright" on mica and "flat" on the highly oriented pyrolytic graphite (HOPG). Our all-atom molecular dynamics simulations reveal that the strong electrostatic interaction induces the "upright" conformation on mica, whereas the hydrophobic interaction favors the "flat" conformation on HOPG. We also show that the epitaxial pattern on mica is ensured by the lattice matching between the anisotropic binding sites of the basal substrate and the molecular dimension of GAV-9, accompanied with a long-range order of well-defined β-strands. Furthermore, the binding free energy surfaces indicate that the longitudinal assembly growth is predominantly driven by the hydrophobic interaction along the longer crystallographic unit cell direction of mica. These findings provide a molecular basis for the surface-assisted molecular assembly, which might also be useful for the design of *de novo* nanodevices.

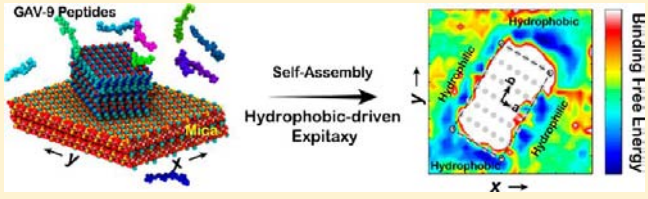

INTRODUCTION

Amyloid fibril has long been recognized as a critical pathogen for a number of progressive neurodegenerative diseases, including Alzheimer's, Parkinson's, and prion diseases. Amyloidosis of peptides is considered as one of most important driving force of these neuron diseases.[1−3] In recent years, the self-assembly properties of the highly ordered amyloid-like peptides on substrate surface have attracted considerable research attentions, with the aim of understanding the disease pathology, as well as exploring potential applications in *de novo* nanodevice design and fabrication.[4] The buildup of the amyloid is controlled not only by the peptide sequence but also by environmental factors such as peptide concentration, pH, ionic strength, temperature, solvent, and surface polarity. The supporting substrate is often believed to be the single most important factor that controls the morphology of the adsorbed assembly.[5,6] For example, the amyloid-β peptide[7] found in Alzheimer's disease shows totally different morphologies on the mica surface or the highly oriented pyrolytic graphite (HOPG) surface, with oligomeric protofibrilar aggregates on the former and elongated assembly along the surface epitaxial order on the latter, respectively.[8,9] On the other hand, the pathogenic protein for Parkinson's disease, α-synuclein (α-syn), prefers sheet growth along the crystalline atomic structure on the mica, but not on the hydrophobic HOPG.[10]

Because of these unique properties, inorganic surfaces, such as mica, have been employed as biomimetic models of cell membranes to study the self-assembly of these important disease-related peptides, particularly their epitaxial growth patterns.[8−10] While the atomic structure of the substrate surface is known to be one of the key factors for assembly,[5,6] the detailed molecular mechanism remains illusive,[10−12] largely due to the current limited experimental resolutions, as well as the inherent dynamic and complex nature of the epitaxial growth. Here we use peptide GAV-9 (NH_3^+-VGGAVVAGV-$CONH_2$),[13] obtained from consensus sequences of the Aβ peptide, α-syn and prion protein (PrP),[14] as an example to study the amyloid-like peptide assembly on both mica and HOPG surfaces with atomic level details.

Our previous *in situ* atomic force microscopy (AFM) showed that the GAV-9 peptide could assemble on both mica and HOPG surfaces, but with very different morphologies. The heights of the peptide nanostructures differ significantly, with 3.0 ± 0.1 nm on mica and 0.9 ± 0.1 nm on HOPG,[13] indicating a potential "upright" conformation on mica and a "flat" conformation on HOPG. In this follow-up study, we use large-scale molecular dynamics (MD) simulations to investigate the

Received: November 7, 2012
Published: January 29, 2013

dx.doi.org/10.1021/ja310989u | J. Am. Chem. Soc. 2013, 135, 3150−3157

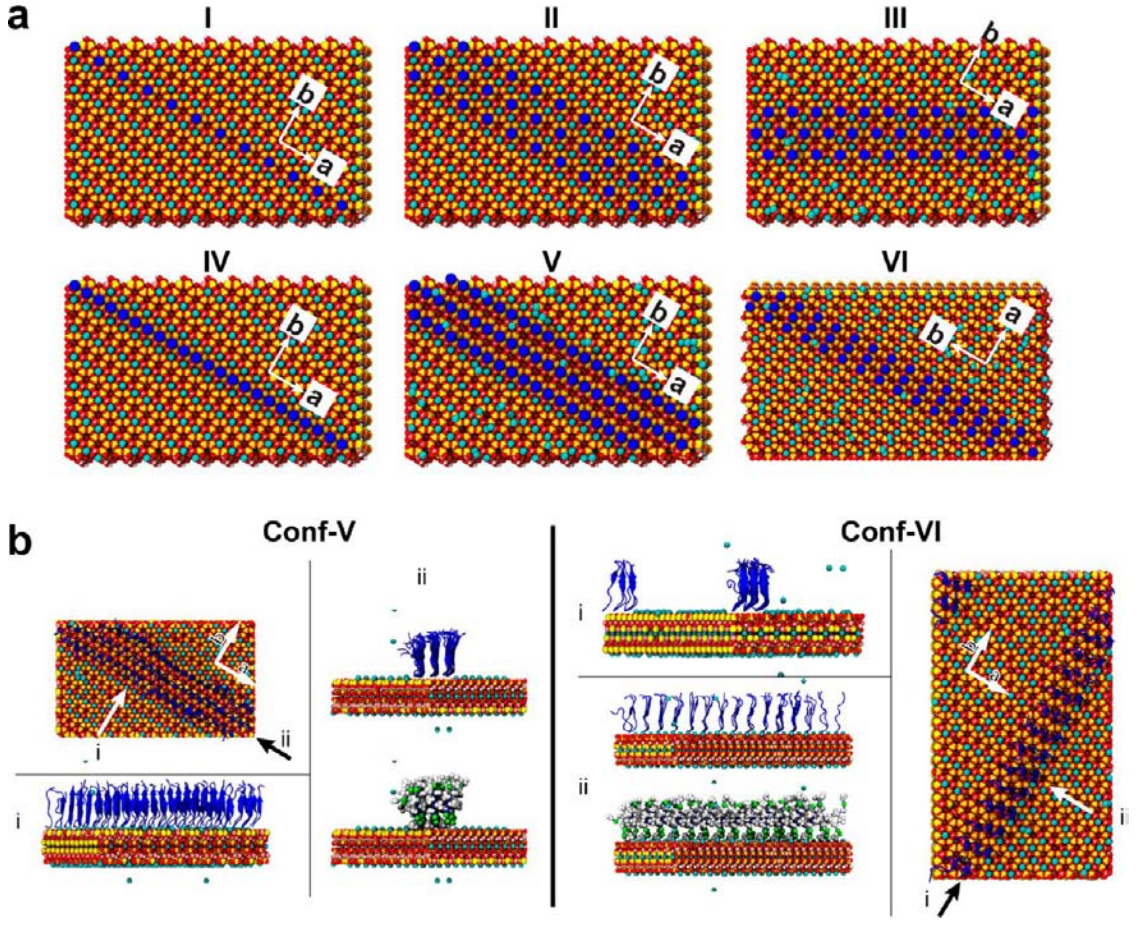

Figure 1. GAV-9 configurations on mica. (a) The GAV-9 peptides are loaded on mica surface depending on surface density, supporting rows and epitaxial direction, where the blue dots display positions of the N-terminal nitrogen atoms of the GAV-9 peptides. The arrows with letters in each configuration indicates the two anisotropic epitaxial binding directions (i.e., *a*- and *b*-directions). (b) Representative structures for the tightly packed **conf-V** and **VI** at the end of the simulations. GAV-9 peptides form stable hydrogen-bonding networks (see viewpoint i) and hydrophobic interactions (see viewpoint ii) along the *a*- and *b*-directions, respectively, where the hydrophobic residues are depicted with white space-filling models.

assembly structure and dynamics of GAV-9 on mica and HOPG with atomic detail. We approach this problem by examining both external (i.e., substrate surfaces and peptide densities) and internal (i.e., physical interactions) factors that control the peptide assembly. We show how these factors work together to generate the epitaxial patterns shown in AFM experiments. Furthermore, a potential epitaxial growth mechanism (growth direction) is presented, with the hydrophobic packing identified as the dominant driving force along the longitudinal growth direction.

■ RESULTS AND DISCUSSION

We carried out MD simulations on the substrate surfaces of both mica and HOPG. The mica surface was constructed with double layered muscovite (001) ($KAl_2(Si_3Al)O_{10}(OH)_2$) using the CLAYFF force field.[15] On the mica surface, there are two crystallographic axes (i.e., *a* and *b*) depending on the distance between the nearest periodic units (centers of Al/Si di-trigonal six-membered tetrahedral rings). Along the crystallographic unit cell, the *a*- and *b*-directions are shorter and longer, with d_a = 0.52 nm and d_b = 0.92 nm, respectively. Each of these directions repeats in every 120°.[16] Since there is no structural information available for the assembly on mica, we configured various possible assembly patterns for our investigation. Figure 1a shows the six different configurations (**conf-I**–**VI**) that were examined. These systems were set up with the peptide packing density increases in the order of **I** = **II** < **III** < **IV** = **V** = **VI**, using 12–72 peptides. In our search, two crystallographic directions of the mica surface have been incorporated for their effect on the epitaxial assembly of the peptides (i.e., **conf-V** vs **VI**). As for comparison, we also set up two systems for HOPG configured with different peptide densities ($\mathbf{I}_{HOPG}$ and $\mathbf{II}_{HOPG}$) as shown in Figure 3 (see detailed rationales below and in the Supporting Information).

Surface Polarity Determines Global Structure of Peptide Self-Assembly. Figures 1b and S1 (Supporting Information) show representative structures at the end of the MD simulations on mica. The GAV-9 peptides remain generally stable at their initially deposited sites on the mica surface despite the low peptide packing density such as in **conf-I**. Interestingly, even in such low concentration as in **conf-I**, the GAV-9 peptides, with their hydrophobic tails moving freely in the water in a random-coiled state, can still maintain a somewhat "standing-up" conformation with an average peptide height of 1.7 ± 0.4 nm and tilt angle of 32 ± 20° from the surface normal (Figure 2). As a control run, we also constructed a system with the same density as **conf-I**, but with peptides initially "lying-down" on mica. These "lying-

dx.doi.org/10.1021/ja310989u | *J. Am. Chem. Soc.* 2013, 135, 3150–3157

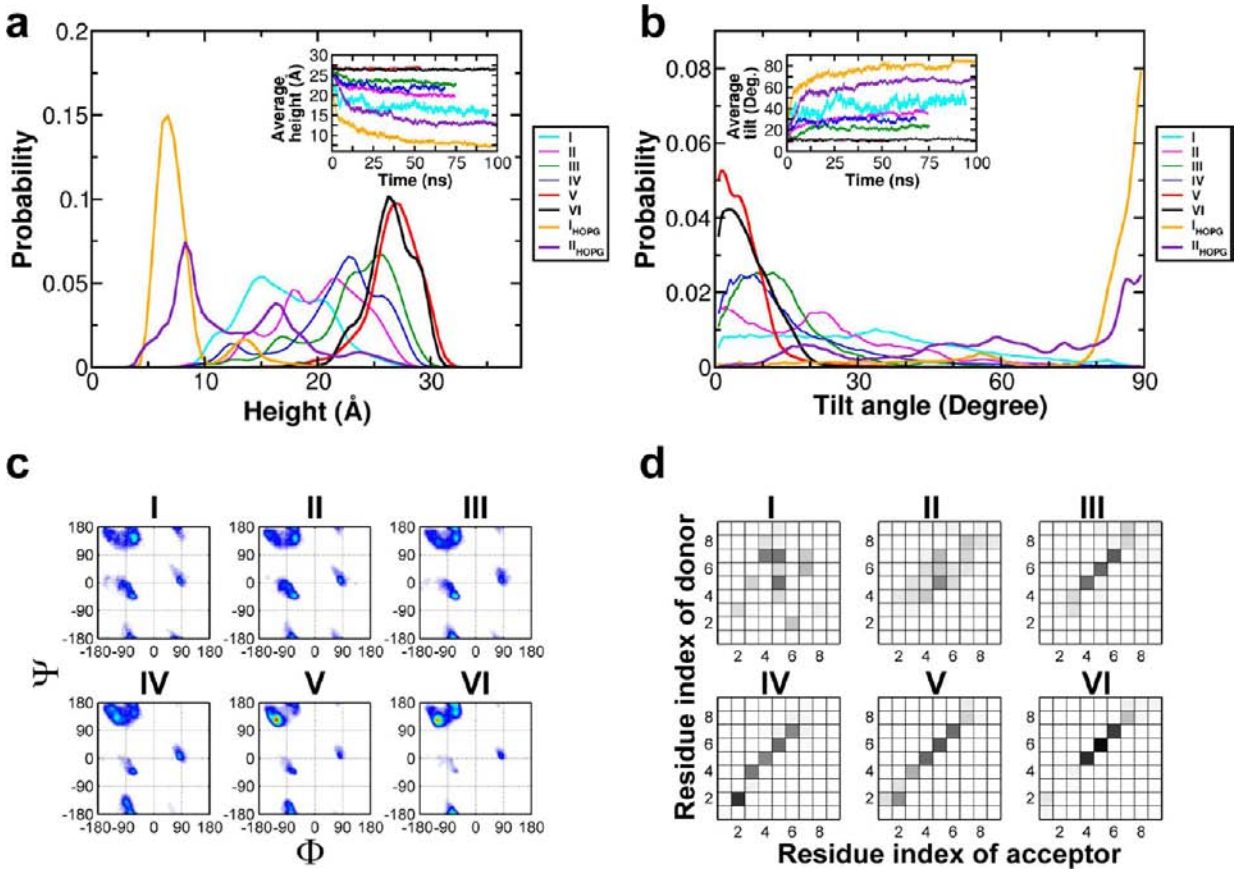

Figure 2. Structural analyses of GAV-9 on mica and HOPG. (a) Height distribution of GAV-9 peptides, where the height is defined as a peptide length projected onto the axis of the surface normal, and time profiles of peptide heights averaged over all chains in each time frame (inset). (b) Tilting angle distribution of GAV-9 peptides, where the tilt angle is defined as angle difference between the principal axis of a peptide and the surface normal, and time profiles on peptide tilting angles averaged over all chains (inset). The distributions are normalized with a sinusoidal distribution function. (c) Ramachandran plots. As the surface density increases, the β-structures becomes significantly dominant (i.e., see population on upper-left corner), where colors spans from white to red to indicate low and high probabilities, respectively. (d) Inter-peptide hydrogen-bonding network. As the surface density increases, the backbone hydrogen bonds between residues of side chains become more probable, resulting in highly ordered β-stranded structures, where color spans from white to black to indicate low and high probabilities, respectively.

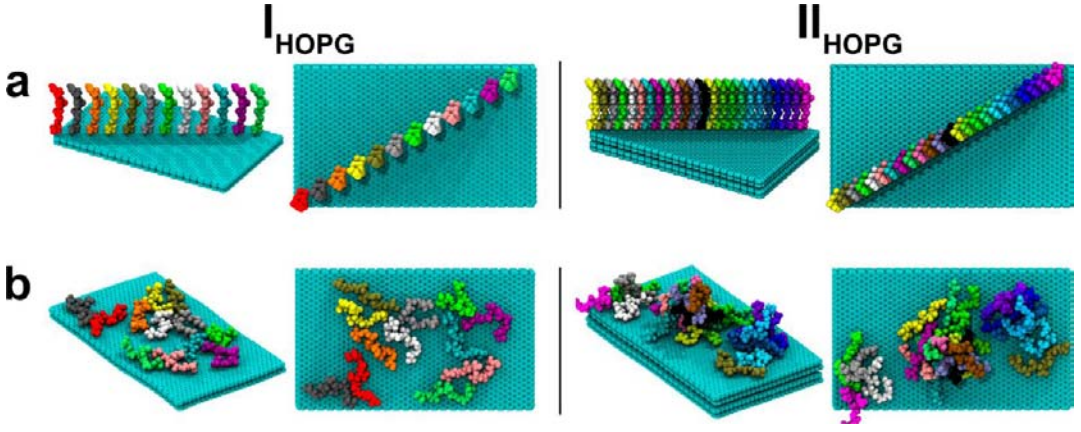

Figure 3. GAV-9 configurations on HOPG. (a) Initial structures of GAV-9 on HOPG. Two surface densities $\mathbf{I}_{HOPG}$ and $\mathbf{II}_{HOPG}$ respectively with 12 and 24 peptides were configured from the "upright" conformation on HOPG surfaces. (b) Representative structures of GAV-9 at the end of the simulations. GAV-9 lied down on HOPG with favorable hydrophobic interaction between the surface and the peptide side chains.

down" peptides quickly evolve to partially "standing-up" conformations (in ~25 ns), converging to similar peptide heights and tilt angles as those found in **conf-I** (Figure S2). This is in distinct contrast with the case of HOPG ($\mathbf{I}_{HOPG}$) with a similar peptide packing density as in **conf-I**, where almost all the GAV-9 peptides end up complete "lying-down" on the surface within 50 ns of simulations, resulting in an average height of <1.0 nm and a tilt angle of ~90° from the surface normal (Figures 2 and 3). The same is also observed in $\mathbf{II}_{HOPG}$, where the peptides are more tightly packed with similar density

dx.doi.org/10.1021/ja310989u | J. Am. Chem. Soc. 2013, 135, 3150−3157

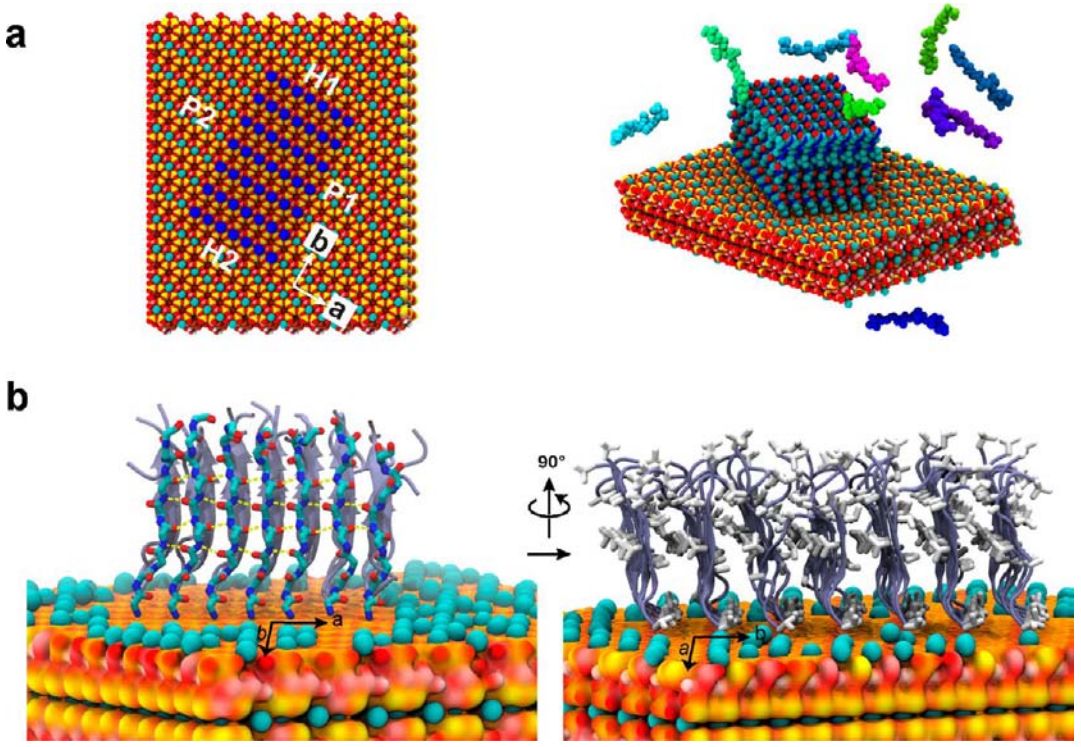

Figure 4. Inter-peptide interactions in epitaxy. (a) Initial configuration of the assembly growth dynamics. The growth dynamics of GAV-9 peptides were examined on a 7×7 peptide island on mica. The hydrophobic and hydrophilic edges are indicated as H1 and H2, and P1 and P2, respectively. (b) The GAV-9 peptides assemble to form highly ordered β-stranded structures. The long-range order is stabilized by bidirectional intermolecular interactions, backbone hydrogen bonds, and side-chain hydrophobic interactions commensurate with anisotropic lattice directions of the basal mica surface.

as in **conf-IV**, although it takes a bit longer before all the peptides start to collapse to the HOPG surface. The low density results are qualitatively consistent with the experimental observation of "upright" conformation on mica and "flat" conformation on HOPG, implying that the surface polarity is indeed one of the intrinsic factors controlling the peptide assembly.

This different peptide conformation can be explained by the fact that GAV-9 contains only hydrophobic side chains except for the charged N-terminus; thus, it would be energetically favorable to lie down on the hydrophobic HOPG surface to maximize the hydrophobic packing. In contrast, for the mica surface, the favorable electrostatic interactions between the positive N-terminal $NH3^+$ and the negatively charged muscovite mica surface play an important role in pinning the positions of GAV-9 even in a sparse packing density, which is consistent with previous experiments that ammonium ion NH_4^+ can replace K^+ on mica surface with high capacity.[17,18] In addition, both experiments[19,20] and theory[21] have previously shown that the charged mica surface creates a highly ordered interfacial water structure, as we have also seen in our hydrophobicity analysis near the surface (see details below and Figure 5). Stabilizing one end of GAV-9 on mica may even increase conformational fluctuations in the rest of the peptide chain. This would make it thermodynamically unfavorable for the hydrophobic chain to adsorb onto the polar mica surface, not to mention that it also needs to overcome the desolvation penalty from the surface hydration shell in doing so. Consequently, the peptide prefers to stay upright, pivoting at the charged N-terminus on the surface.

Surface Lattice Structure Controls Epitaxial Assembly of GAV-9. To gain a deeper insight at the molecular level into the quantitative behavior found in the AFM experiments on mica (i.e., ∼3.0 nm height),[13] we have performed MD simulations with additional supporting rows of peptides (**conf-II**) as well as slightly increased peptide density (**conf-III**). However, these configurations only result in a slight improvement where the peptides stand up with a height and tilt angle of (∼2.0 nm, ∼23°), and (∼2.3 nm, ∼14°), as seen in **conf-II** and **conf-III**, respectively (Figure 2). On the other hand, we start to observe the formation of secondary structures during the process, even though it happens only transiently and locally (Figure S1). This motivates us to investigate additional systems with higher peptide density thus tighter packed structures (i.e., **conf-IV**, **V**, and **VI**).

In **conf-IV**, the peptides were placed on every possible (i.e., nearest neighbor) epitaxial site along the *a*-direction in a single row. Initially this configuration was infeasible due to the extremely tight dimension match between the peptide width (∼1 nm) and the binding site separation ($d_a \approx 0.5$ nm). This problem was later solved by stretching out the bulky hydrophobic side chains of the peptides toward the less crowded side line (i.e., *b*-direction), thus leaving only backbone atoms in the longitudinal axis of the assembly line (i.e., *a*-direction) in order to accommodate the peptides. For this system, the peptides result in a better upright position of ∼2.2 nm height and ∼17° tilt angle, even without any supporting rows (Figure S1). However, this arrangement has a slight drawback from energetic point of view, including (i) sequestration of the hydrophilic backbone atoms from water, and also (ii) exposure of the hydrophobic side chains to water.

dx.doi.org/10.1021/ja310989u | J. Am. Chem. Soc. 2013, 135, 3150−3157

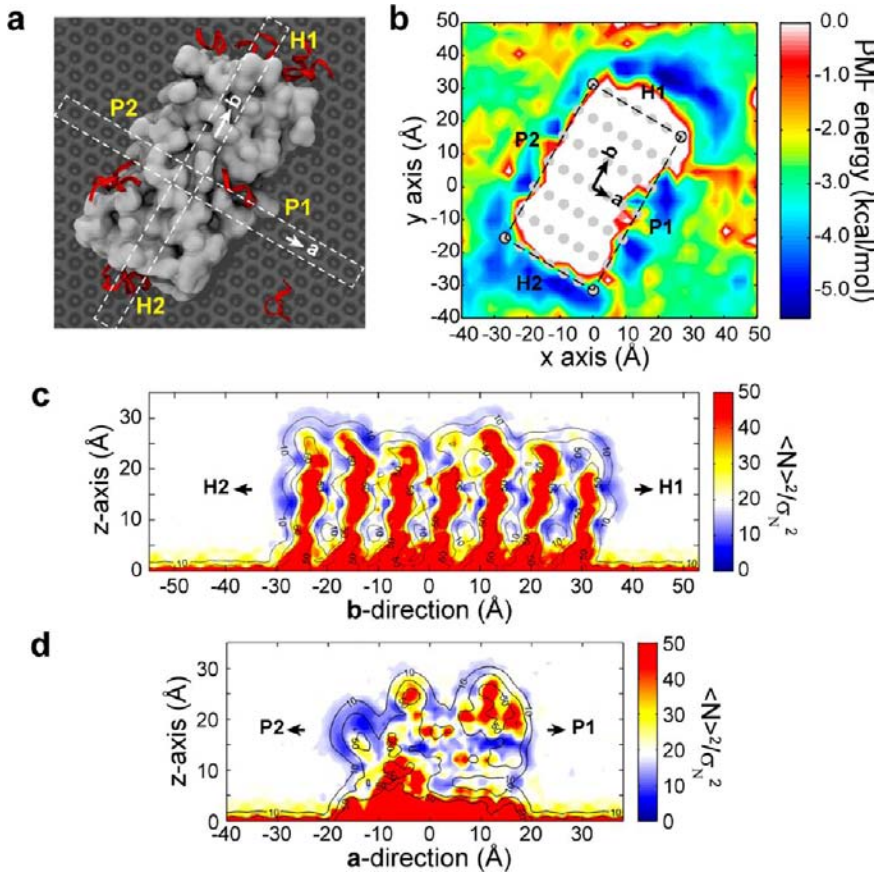

Figure 5. Growth dynamics of GAV-9 assembly. (a) Representative snapshot at the end of GAV-9 binding simulations. The snapshot shows that GAV-9 preferentially bind to the hydrophobic H1 and H2 edges. (b) Binding free energy surface around the 7×7 GAV-9 island. The potential of mean force analysis reveals that both hydrophobic H1 and H2 edges are more favorable to interact with GAV-9 monomers, implying the *b*-direction prevails over the *a*-direction for the longitudinal direction of the epitaxial pattern. (c,d) Hydrophobicity analysis over the four edges. The inverse normalized density fluctuation reveals that both H1 are H2 interfaces are highly fluctuating, which ensures that the assembly growth is dominantly driven by hydrophobic interaction, and shows that the growth is bidirectional. The yellow colors above the mica surface indicate an enhancement of ordered water structures due to the surface polarity. The contour lines indicate the number densities of solute and surface atoms in the interaction region.

To overcome these two shortcomings, the former could be compensated by the intermolecular hydrogen bond as shown in the global enhancement of the secondary structures (Figure S1d), and the later could be resolved by additional rows (detailed discussion below).

In **conf-V**, two adjacent parallel supporting rows were added to the central single row (by the unit distance of d_b = 0.92 nm). For this system, our simulations show that almost all the peptides are involved in the long-range β-stranded structure from the very beginning of the simulations, albeit started with arbitrary elongated conformation (Figure 1b). The resulting position of the peptides is improved dramatically to a height of 2.7(±0.2) nm and a tilt angle of 6(±5°), in excellent agreement with the AFM experiments. Finally, in **conf-VI**, we populated the peptides with the same density as in **conf-V** but grew them along the *b*-direction. Our simulations show a height of 2.6(±0.2) nm and a tilt angle of 7(±5)° (Figure 1b), which is also remarkably consistent with the AFM experiments. In addition, the radius of gyration (R_g) also revealed similar results (Figure S3). With the increase of the peptide density on mica (i.e., **conf-V** and **VI**), the average R_g increases and its distribution width narrows. In other words, it is more likely for the peptides to have elongated conformations as their packing density increases. This is attributed to the favorable desolvation incorporated with the highly organized β-sheet formation via stable interchain hydrogen bond and hydrophobic interaction along with the crystallographic *a*- and *b*-directions, respectively (more details below).

Similar to **conf-IV**, the GAV-9 peptides in both **conf-V** and **VI** are able to construct an efficient hydrogen-bonding network along the *a*-direction through the polar backbone atoms (i.e., Figure 4b). At the same time, the bulky hydrophobic side chains make a favorable knob-and-hole type of van der Waals interactions along the *b*-direction (i.e., Figure 4b). This serves to bury the hydrophobic side chains from the solvent and form more stable β-stranded structures than the single-row **conf-IV**. Figure 2c,d shows the analyses on the backbone dihedral angles and the hydrogen bonds, which summarize the interplay between the density of the peptides and their structural integrity. From these analyses it is clear that peptides are more ordered with increasing stable β-strands in the tightly packed configurations (i.e., **conf-IV**, **V**, and **VI**), whereas in the loosely packed configurations they are more likely to be in random coils (i.e., **conf-I**, **II**, and **III**) even when they are bound to the substrate surface. These findings indicate the substrate structure, intertwined with intrinsic physical inter-peptide interactions,[22] could effectively control the peptide self-assembly.

dx.doi.org/10.1021/ja310989u | *J. Am. Chem. Soc.* 2013, 135, 3150−3157

Our study reveals that the lattice matching between the two-dimensional (2D) anisotropies of the mica surface and the β-stranded peptide network plays a crucial role in controlling the ordered self-assembly on mica. Quantitative measurements indicate that the anisotropic binding sites along the *a*- and *b*-directions are separated by ∼0.5 and ∼0.9 nm, respectively, which matches almost perfectly to the inter-peptide hydrogen bond distance (∼0.48 nm along the *a*-direction) and the face-to-face distance (∼1 nm along the *b*-direction) between the neighboring peptides with a β-structure.[23] It is this near perfect match in mica lattice size that greatly facilitated both the peptide epitaxial adsorption and the highly ordered structural formation, in addition to the surface chemistry (strong electrostatic interactions between the peptide N-terminus and mica surface negative cavity).

Hydrophobic Packings Drive Epitaxial Growth Direction. Despite both satisfactory results from **conf-V** and **VI** as compared to AFM experiment, it is still not clear whether the peptide assembly prefers to grow in the *a*- or the *b*-direction. To further investigate this growth mechanism, we devised a system consisting of an island of 7×7 GAV-9 peptides pre-adsorbed on the mica surface, plus 10 individual peptides randomly distributed in solvent (Figure 4a), which will be monitored for their interactions (adsorptions) with the GAV-9 island especially at its four exposed edges. This in turn will help determine the epitaxial growth direction on mica. Figure 5a,b shows one representative snapshot and a potential of mean force (PMF) surface for the individual peptide interaction with the pre-adsorbed island, respectively. The PMF was calculated by the histogramming analysis,[24,25] using the equation $w(x,y) = -RT \ln p(x,y)$, where $p(x,y)$ is the probability for peptides to be found in a position (x,y) on the mica surface (measured with their center-of-mass positions), with five independent runs, each with at least 200 ns-long trajectory. The PMF reveals that the GAV-9 peptides are more likely to interact with the peptide island in the H1 and H2 edges (hydrophobic edges), rather than P1 and P2 ones (hydrophilic edges) (see Figure 5). This reveals that (i) the *b*-direction is the energetically more favorable growth direction than the *a*-direction, and (ii) the assembly growth is bi-directional along the *b*-direction (i.e., growing at both H1 and H2 fronts symmetrically), which supports our early observations in the AFM experiment.[13] On the other hand, the P1 and P2 fronts are asymmetric along the *a*-direction, with P1 side more favorable in term of binding affinity (Figure 5b), largely due to its dangling backbone H-bonds to the incoming peptides (more discussions below). In addition to the 2D PMF, the 1D PFM along the normal direction from each front gives a consistent result that the hydrophobic fronts have more favorable interaction with the incoming peptides than the hydrophilic fronts do (Figure S4). Interestingly, the optimal distances found at the energy minima in 1D PMF match very well with the epitaxial binding distances to the corresponding directions.

In the following analysis, the hydrophobicity of each edge has been estimated by calculating the inverse normalized density fluctuations $(\langle N\rangle^2/\sigma_N^2)$[26,27] over all heavy atoms within a methane-sized cavity of radius of 0.33 nm in every 0.1 nm grid, over the two orthogonal cross sections passing through the island along *a*- and *b*-directions, respectively (see dashed boxes in Figure 5a). The $\langle N\rangle$ and σ_N^2 denote the ensemble average of the number of heavy atoms, and the number fluctuation $(\langle N^2\rangle - \langle N\rangle^2)$ in the cavity, respectively. The hydrophobicity has previously been shown to correlate with the local compressibility of a molecular-sized volume near the hydration shell based on density fluctuation $(\sigma_N^2/\langle N\rangle^2)$.[26,27] The inverse density fluctuation is approximately proportional to the excess free energy $(\mu^{ex} \approx (kT/2)(\langle N\rangle^2/\sigma_N^2))$ for generating a methane-sized cavity,[28,29] where k is Boltzmann's constant and T is temperature. As such, compared to the bulk water, the quantity $\langle N\rangle^2/\sigma_N^2$ at a given interface indicates the necessary work to create a methane-sized cavity at the interface, with (i) a low value (i.e., more compressible) near the hydrophobic surface, and (ii) a high value (i.e., less compressible) near the hydrophilic surface.

Figure 5c shows that both *b*-directional edges H1 and H2 are highly hydrophobic. This presents a rationale on the aforementioned PMF result that the high contact probability on H1 and H2 are predominantly driven by the hydrophobic interactions (hydrophobic packing). On the other hand, P1 and P2 are characterized to be relatively more hydrophilic (Figure 5d), and they are asymmetric where P1 side is more favorable in term of PMF affinity, as mentioned above, due to backbone H-bonds with incoming peptides. The slightly more hydrophobic character of P2 is related to the frequent exposure of hydrophobic side chains and its effect on surface curvature. Based on the PMF and density fluctuation results, we can propose a mechanism for the epitaxial growth on mica. The GAV-9 peptides assemble bi-directionally (i.e., both H1 and H2 fronts) along the *b*-direction through strong hydrophobic packings, similar to the hydrophobic collapses in protein folding,[9,30−32] where many recent studies have shown that maintaining a dry hydrophobic core is crucial for protein stability. The nanoscale drying (or dewetting) within the hydrophobic core or patch provides a significant driving force for the folding and collapse of both physical and biological systems.[33−39] Thus, our current findings clearly indicate that the *b*-direction is the preferred longitudinal growth direction for the assembly, making **conf-VI** a more representative structure. Meanwhile, the contact on more hydrophilic P1 and P2 edges may contribute to the transversal (width) growth along the *a*-direction, albeit less favorable due to the relatively high desolvation penalty when removing the hydration shell around the polar backbones.[22] Indeed, the *in situ* AFM images showed that the average width of the GAV-9 fibrils on mica is ∼12 nm after deconvolution[13] which means there exist about 24 layers of GAV-9 along the transversal direction, considering the epitaxial binding distance of ∼0.5 nm along this crystallographic *a*-direction.

■ CONCLUSIONS

To conclude, we investigated the molecular mechanism of the self-assembly of an amyloid-like nine-residue GAV-9 peptide which has shown linear epitaxial patterns on the polar mica and nonpoloar HOPG surfaces. Using atomistic molecular dynamics simulations, we found that the surface polarity determines the global morphologies of GAV-9, "upright" on mica and "flat" on HOPG, even with relatively low surface peptide density. The lattice structure (i.e., *a*- and *b*-directions) of the mica surface are commensurate with the molecular dimension of the peptides, which induces a highly ordered β-stranded structure with synergies from both the backbone hydrogen bondings and the side-chain hydrophobic packings along the surface crystallographic *a*- and *b*-directions, respectively. On the assembly growth mechanism, the binding interaction between the 7×7 peptide island and the GAV-9 monomers ascertained the dominant role of the hydrophobic packings, thus suggesting

the *b*-directional growth to be the longitudinal axis of the GAV-9 epitaxy on mica.

Our simulations reveal both static structures and dynamic processes on the peptide self-assembly on a highly ordered surface such as mica with atomic details. We believe that our findings would serve as a theoretical background for better understanding of the surface-assisted molecular assembly and future design of highly ordered *de novo* nanodevices.

SYSTEMS AND METHODS

In our MD simulations, the two substrates, mica and HOPG, were prepared as following. For mica, we applied the Al-avoidance or Loewenstein's rule[40,41] and based on the monoclinic $C2/c$ $2M_1$ crystal structure[16] to construct the mica surface using double layered muscovite (001) ($KAl_2(Si_3Al)O_{10}(OH)_2$) with the CLAYFF force field.[15] As for HOPG, we used multiple layers of graphene sheets with the CHARMM22 force field.[42]

To facilitate our investigation of the control mechanism of the mica surface on the peptide assembly, we configured six different systems (**conf-I**–**VI**) depending on the surface density, supporting rows and growth direction (Figure 1a). For **conf-I** and **II**, they both have the same linear densities where the peptides are placed in every alternative epitaxial binding site. The only difference is that **conf-II** has two supporting rows with 12 peptides aligned in each row along the *a*-direction. In **conf-III**, the linear packing density is increased by arranging the same number of peptides as in **conf-II** (i.e., 36 chains) along the *x*-axis (i.e., *b*-direction) with loosely packed supporting rows. For **conf-VI**, the packing density is doubled to that of **conf-i**, as there are 24 peptides tightly packed along the *a*-direction and placed in every possible epitaxial binding site. For **conf-V** (72 peptides) and **VI** (48 peptides), they both have the same surface densities as in **conf-IV**; however, these two last systems have different growth directions. The CHARMM22 (c32b1 parameter set) force field[42] was used for the description of the GAV-9 peptides. The compatibility of the CLAYFF and CHARMM force fields has been studied extensively, and reasonable agreements with experiment have been found previously.[43−47] All six systems were solvated in the water boxes with 12 000−17 000 TIP3P[48] water molecules. To ensure the linear assembly over the periodic boundary condition, the surface area of **conf-I**–**V** is set to 107.6 × 63.8 Å^2, whereas for **conf-VI**, it is set to 71.8 × 127.7 Å^2. As for comparisons, we also set up two HOPG systems with different densities, one low ($\mathbf{I}_{HOPG}$; 12 peptides) and one high ($\mathbf{II}_{HOPG}$; 24 peptides), on a 109.5 × 65.5 Å^2 HOPG surface (Figure 3). These two systems were solvated in the water boxes with ∼12, 000 TIP3P water molecules.

To study the assembly growth mechanism, we also prepared a system containing an assembly seed which is a 7×7 island of GAV-9 peptides tightly packed as in **conf-V** or **VI** and loaded on a 89.7 × 106.4 Å^2 mica surface. In addition, 10 individual GAV-9 peptides were placed in random positions around the seed island without any contact to each other and the island seed. The entire system was solvated in a water box with ∼18 000 TIP3P water molecules (Figure 4a). Five independent simulations were carried out, each with the 10 individual GAV-9 peptides in different random initial configurations.

For all of our MD simulations, we used the NAMD2 package[49] compiled on the IBM Bluegene computer.[50] MD simulations have been widely used to complement experiments,[51−62] which can provide atomic details that are often inaccessible in experiments due to resolution limits, even with the currently available sophisticated experimental techniques. The Particle Mesh Eward method[63] was applied to treat the long-range electrostatic interactions and a 12.0 Å cutoff was used to handle the nonbonding dispersion energies. Before the production run, each system was first minimized for 20 000 steps to remove the bad contacts. The minimized system was then equilibrated for 0.5 ns with a 0.5 fs time step in the NPT ensemble at 1 atm and 310 K. All production runs were performed with 2 fs time step in the same pressure and temperature used in the equilibration. For the systems **conf-I**–**VI**, the simulation lasted from 50 to 100 ns, whereas for HOPG, each run was at least 100 ns long. No special constraints were utilized for holding the peptide fixed, and they were allowed to move freely on each surface with only nonbonded interactions. As for the assembly growth simulations, each trajectory runs for at least 200 ns in order to construct the binding free energy surface.

ASSOCIATED CONTENT

Supporting Information

A more complete description of the muscovite (001) surface construction, PMF, and inverse normalized density fluctuation; Figure S1, representative configuration structures from MD simulations; Figure S2, structural evolution of GAV-9 peptides with two different initial conformations on mica; Figure S3, R_g of GAV-9 peptides; Figure S4, 1D PMF for GAV-9 binding on four edges of the 7×7 GAV-9 island; Figure S5, details of the muscovite (001) mica surface construction. This material is available free of charge via the Internet at http://pubs.acs.org.

AUTHOR INFORMATION

Corresponding Author

ruhongz@us.ibm.com; zhangyi@sinap.ac.cn

Notes

The authors declare no competing financial interest.

ACKNOWLEDGMENTS

We thank Bruce J. Berne, Bo Zhou, and Jun Hu for helpful discussions. We also thank Royce W. Zhou, Matteo Castelli, and Raul Araya for critical reading of the manuscript. R.Z. acknowledges support from IBM Blue Gene Science Program and Fudan University through the Senior Visiting Scholar Grant. G.W. acknowledges financial support from the NSF of China (Grant No. 91227102). Y.Z. thanks the National Basic Research Program of China (2013CB932800) and the National Natural Science Foundation of China (No. 11274334) for support.

REFERENCES

(1) Chiti, F.; Dobson, C. M. *Annu. Rev. Biochem.* **2006**, *75*, 333−366.
(2) Butterfield, S. M.; Lashuel, H. A. *Angew. Chem., Int. Ed.* **2010**, *49*, 5628−5654.
(3) Murphy, R. M. *Biochim. Biophys. Acta* **2007**, *1768*, 1923−1934.
(4) Cherny, I.; Gazit, E. *Angew. Chem., Int. Ed.* **2008**, *47*, 4062−4069.
(5) Yang, H.; Fung, S. Y.; Pritzker, M.; Chen, P. *J. Am. Chem. Soc.* **2007**, *129*, 12200−12210.
(6) Whitehouse, C.; Fang, J. Y.; Aggeli, A.; Bell, M.; Brydson, R.; Fishwick, C. W. G.; Henderson, J. R.; Knobler, C. M.; Owens, R. W.; Thomson, N. H.; Smith, D. A.; Boden, N. *Angew. Chem., Int. Ed.* **2005**, *44*, 1965−1968.
(7) Krone, M. G.; Hua, L.; Soto, P.; Zhou, R.; Berne, B. J.; Shea, J. E. *J. Am. Chem. Soc.* **2008**, *130*, 11066−11072.
(8) Kellermayer, M. S. Z.; Karsai, A.; Benke, M.; Soos, K.; Penke, B. *Proc. Natl. Acad. Sci. U.S.A.* **2008**, *105*, 141−144.
(9) Kowalewski, T.; Holtzman, D. M. *Proc. Natl. Acad. Sci. U.S.A.* **1999**, *96*, 3688−3693.
(10) Hoyer, W.; Cherny, D.; Subramaniam, V.; Jovin, T. M. *J. Mol. Biol.* **2004**, *340*, 127−139.
(11) Yang, G.; Woodhouse, K. A.; Yip, C. M. *J. Am. Chem. Soc.* **2002**, *124*, 10648−10649.
(12) Brown, C. L.; Aksay, I. A.; Saville, D. A.; Hecht, M. H. *J. Am. Chem. Soc.* **2002**, *124*, 6846−6848.
(13) Zhang, F.; Du, H. N.; Zhang, Z. X.; Ji, L. N.; Li, H. T.; Tang, L.; Wang, H. B.; Fan, C. H.; Xu, H. J.; Zhang, Y.; Hu, J.; Hu, H. Y.; He, J. H. *Angew. Chem., Int. Ed.* **2006**, *45*, 3611−3613.

(14) Du, H. N.; Li, H. T.; Zhang, F.; Lin, X. J.; Shi, J. H.; Shi, Y. H.; Ji, L. N.; Hu, J.; Lin, D. H.; Hu, H. Y. *FEBS Lett* **2006**, *580*, 3657−3664.
(15) Cygan, R. T.; Liang, J. J.; Kalinichev, A. G. *J. Phys. Chem. B* **2004**, *108*, 1255−1266.
(16) Kuwahara, Y. *Phys. Chem. Miner.* **1999**, *26*, 198−205.
(17) Osman, M. A.; Suter, U. W. *J. Colloid Interface Sci.* **2000**, *224*, 112−115.
(18) Nock, S.; Spudich, J. A.; Wagner, P. *FEBS Lett.* **1997**, *414*, 233−238.
(19) Cheng, L.; Fenter, P.; Nagy, K. L.; Schlegel, M. L.; Sturchio, N. C. *Phys. Rev. Lett.* **2001**, 87.
(20) Xu, K.; Cao, P.; Heath, J. R. *Science* **2010**, *329*, 1188−1191.
(21) Odelius, M.; Bernasconi, M.; Parrinello, M. *Phys. Rev. Lett.* **1997**, *78*, 2855−2858.
(22) Knowles, T. P.; Fitzpatrick, A. W.; Meehan, S.; Mott, H. R.; Vendruscolo, M.; Dobson, C. M.; Welland, M. E. *Science* **2007**, *318*, 1900−1903.
(23) Serpell, L. C. *Biochim. Biophys. Acta* **2000**, *1502*, 16−30.
(24) Zuo, G.; Huang, Q.; Wei, G.; Zhou, R.; Fang, H. *ACS Nano* **2010**, *4*, 7508−7514.
(25) Zhou, R.; Berne, B. J.; Germain, R. *Proc. Natl. Acad. Sci. U.S.A.* **2001**, *98*, 14931−14936.
(26) Acharya, H.; Vembanur, S.; Jamadagni, S. N.; Garde, S. *Faraday Discuss* **2010**, *146*, 353−365 ; discussion 367-93, 395-40.
(27) Godawat, R.; Jamadagni, S. N.; Garde, S. *Proc. Natl. Acad. Sci. U.S.A.* **2009**, *106*, 15119−15124.
(28) Garde, S.; Hummer, G.; Garcia, A. E.; Paulaitis, M. E.; Pratt, L. R. *Phys. Rev. Lett.* **1996**, *77*, 4966−4968.
(29) Hummer, G.; Garde, S.; Garcia, A. E.; Pratt, L. R. *Chem. Phys.* **2000**, *258*, 349−370.
(30) Liu, P.; Huang, X.; Zhou, R.; Berne, B. J. *Nature* **2005**, *437*, 159−162.
(31) Zhou, R. *Proc. Natl. Acad. Sci. U.S.A.* **2003**, *100*, 13280−13285.
(32) Zhou, R.; Huang, X.; Margulis, C. J.; Berne, B. J. *Science* **2004**, *305*, 1605−1609.
(33) Young, T.; Hua, L.; Huang, X. H.; Abel, R.; Friesner, R.; Berne, B. J. *Proteins* **2010**, *78*, 1856−1869.
(34) Levy, Y.; Onuchic, J. N. In *Annual Reviews in Biophysics and Biomolecular Structures*; Annual Reviews: Palo Alto, 2006; Vol. *35*, pp 389−415.
(35) Berne, B. J.; Weeks, J. D.; Zhou, R. H. In *Annual Reviews in Physical Chemistry*; Annual Reviews: Palo Alto, 2009; Vol. *60*, pp 85−103.
(36) Yang, Z. X.; Shi, B. Y.; Lu, H. J.; Xiu, P.; Zhou, R. H. *J. Phys. Chem. B* **2011**, *115*, 11137−11144.
(37) Wu, Y.; Vadrevu, R.; Kathuria, S.; Yang, X.; Matthews, C. R. *J. Mol. Biol.* **2007**, *366*, 1624−1638.
(38) Eleftheriou, M.; Germain, R. S.; Royyuru, A. K.; Zhou, R. *J. Am. Chem. Soc.* **2006**, *128*, 13388−13395.
(39) Li, X.; Li, J.; Eleftheriou, M.; Zhou, R. *J. Am. Chem. Soc.* **2006**, *128*, 12439−12447.
(40) Loewenstein, W. *Am. Mineral.* **1954**, *39*, 92−96.
(41) Brigatti, M. F.; Guggenheim, S. *Micas: Cryst. Chem. Metamorph. Petrol.* **2002**, *46*, 1−97.
(42) MacKerell, A. D.; Bashford, D.; Bellott, M.; Dunbrack, R. L.; Evanseck, J. D.; Field, M. J.; Fischer, S.; Gao, J.; Guo, H.; Ha, S.; Joseph-McCarthy, D.; Kuchnir, L.; Kuczera, K.; Lau, F. T. K.; Mattos, C.; Michnick, S.; Ngo, T.; Nguyen, D. T.; Prodhom, B.; Reiher, W. E.; Roux, B.; Schlenkrich, M.; Smith, J. C.; Stote, R.; Straub, J.; Watanabe, M.; Wiorkiewicz-Kuczera, J.; Yin, D.; Karplus, M. *J. Phys. Chem. B* **1998**, *102*, 3586−3616.
(43) Payne, C. M.; Zhao, X.; Vlcek, L.; Cummings, P. T. *J. Phys. Chem. B* **2008**, *112*, 1712−1717.
(44) Heine, D. R.; Rammohan, A. R.; Balakrishnan, J. *Mol. Simul.* **2007**, *33*, 391−397.
(45) Swadling, J. B.; Coveney, P. V.; Greenwell, H. C. *J. Am. Chem. Soc.* **2010**, *132*, 13750−13764.
(46) Skelton, A. A.; Fenter, P.; Kubicki, J. D.; Wesolowski, D. J.; Cummings, P. T. *J. Phys. Chem. C* **2011**, *115*, 2076−2088.
(47) Kang, S. G.; Li, H.; Huynh, T.; Zhang, F.; Xia, Z.; Zhang, Y.; Zhou, R. *ACS Nano* **2012**, *6*, 9276−9282.
(48) Jorgensen, W. L.; Chandrasekhar, J.; Madura, J. D.; Impey, R. W.; Klein, M. L. *J. Chem. Phys.* **1983**, *79*, 926−935.
(49) Phillips, J. C.; Braun, R.; Wang, W.; Gumbart, J.; Tajkhorshid, E.; Villa, E.; Chipot, C.; Skeel, R. D.; Kale, L.; Schulten, K. *J. Comput. Chem.* **2005**, *26*, 1781−1802.
(50) Kumar, S.; Huang, C.; Zheng, G.; Bohm, E.; Bhatele, A.; Phillips, J. C.; Yu, H.; Kale, L. V. *IBM J. Res. Dev.* **2008**, *52*, 177−188.
(51) Brooks, C. L.; Gruebele, M.; Onuchic, J. N.; Wolynes, P. G. *Proc. Natl. Acad. Sci. U.S.A.* **1998**, *95*, 11037−11038.
(52) Brooks, C. L.; Onuchic, J. N.; Wales, D. J. *Science* **2001**, *293*, 612−613.
(53) Fersht, A. R.; Daggett, V. *Cell* **2002**, *108*, 573−582.
(54) Snow, C. D.; Nguyen, N.; Pande, V. S.; Gruebele, M. *Nature* **2002**, *420*, 102−106.
(55) Garcia, A. E.; Onuchic, J. N. *Proc. Natl. Acad. Sci. U.S.A.* **2003**, *100*, 13898−13903.
(56) Kokubo, H.; Okamoto, Y. *Chem. Phys. Lett.* **2004**, *383*, 397−402.
(57) Zhou, R.; Berne, B. J. *Proc. Natl. Acad. Sci. U.S.A.* **2002**, *99*, 12777−12782.
(58) Zhou, R.; Eleftheriou, M.; Royyuru, A. K.; Berne, B. J. *Proc. Natl. Acad. Sci. U.S.A.* **2007**, *104*, 5824−5829.
(59) Hua, L.; Zhou, R.; Thirumalai, D.; Berne, B. J. *Proc. Natl. Acad. Sci. U.S.A.* **2008**, *105*, 16928−16933.
(60) Ge, C.; Du, J.; Zhao, L.; Wang, L.; Liu, Y.; Li, D.; Yang, Y.; Zhou, R.; Zhao, Y.; Chai, Z.; Chen, C. *Proc. Natl. Acad. Sci. U.S.A.* **2011**, *108*, 16968−16973.
(61) Kang, S. G.; Zhou, G.; Yang, P.; Liu, Y.; Sun, B.; Huynh, T.; Meng, H.; Zhao, L.; Xing, G.; Chen, C.; Zhao, Y.; Zhou, R. *Proc. Natl. Acad. Sci. U.S.A.* **2012**, *109*, 15431−15436.
(62) Xia, Z.; Das, P.; Shakhnovich, E. I.; Zhou, R. *J. Am. Chem. Soc.* **2012**, *134*, 18266−18274.
(63) Darden, T.; York, D.; Pedersen, L. *J. Chem. Phys.* **1993**, *98*, 10089−10092.